Comparison of Boundary Layer Similarity Transformations for High Mach Number Flows

Nicholas J. DiGregorio* and Tomasz G. Drozda†
NASA Langley Research Center, Hampton, VA, 23681, USA

Cyrus K. Madnia‡
State University of New York at Buffalo, Buffalo, NY, 14260, USA

Reynolds averaged Navier-Stokes (RANS) simulations of the turbulent boundary layer flow on a flat plate are performed across a Mach number range of 0.3 up to 16 using the computational fluid dynamics (CFD) software, VULCAN-CFD. The simulation results are used to evaluate the ability of the Van Driest transformation and the transformation of Trettel and Larsson to collapse boundary layer velocity profiles under various flow conditions across the range of Mach numbers. The flat plate wall boundary conditions and leading edge geometry are varied from adiabatic to isothermal and sharp to blunted to reveal the physics of how these effects impact the performance of the chosen flow transformations. Results indicate that the transformation of Trettel and Larsson produces a better collapse of velocity profile data than the Van Driest transformation regardless of Mach number, wall boundary condition, or leading edge geometry. In addition, the velocity gradients obtained from the transformation of Trettel and Larsson match the normalized untransformed velocity gradients much more closely than those obtained using the Van Driest transformation.

I. Introduction

Hypersonic flight has been achieved many times, both by rocket-based and air-breathing systems, but many questions still remain. In addition to the propulsion, structural, and material challenges, some aerothermodynamic analysis techniques break down at the high speeds and rates of heat transfer encountered in hypersonic flight. Among these techniques is the law of the wall [1] and its compressible extension, the Van Driest transformation [2, 3], which often fail to collapse turbulent boundary layer velocities to a single universal profile. This concept of collapsing profiles is referred to as self-similarity.

The logarithmic law of the wall is an empirical relationship that results from dimensional analysis and matching the velocity profiles in the viscous sublayer and the defect layer [4]. This scaling law allows the velocity profiles within incompressible boundary layers to be collapsed onto a single profile, thereby obtaining self-similarity. The law of the wall for incompressible flows [5] uses the scaled wall-normal coordinate, y^+, to give the scaled velocity, u^+, as

$$u^+ = \frac{u}{u_\tau} = \frac{1}{\kappa_c} ln(y^+) + C, \tag{1}$$

$$y^+ = \frac{\rho_w u_\tau y}{\mu_w}, \tag{2}$$

where u is the streamwise velocity component, y is the wall-normal distance, κ_c is von Kármán's constant, C is a dimensionless constant, and u_τ is the friction velocity

$$u_\tau = \sqrt{\frac{\tau_w}{\rho_w}}, \tag{3}$$

with the wall shear stress

$$\tau_w = \mu_w \left.\frac{\partial u}{\partial y}\right|_w, \tag{4}$$

*Aerospace Engineer, Vehicle Analysis Branch, AIAA Member.
†Research Aerospace Engineer, Hypersonic Airbreathing Propulsion Branch, AIAA Associate Fellow.
‡Professor of Mechanical and Aerospace Engineering, Department of Mechanical and Aerospace Engineering, AIAA Associate Fellow.

where ρ is the density, μ is the dynamic viscosity, and the subscript w denotes a quantity at the wall. Experiments indicate that $\kappa_c \approx 0.41$ and $C \approx 5.2$, but as stated by Pope [5], "there is some variation in the values ascribed to the log-law constants, but generally they are within 5%" of the values stated above. Although the law of the wall successfully collapses velocity profiles for incompressible flows, it does not scale velocities correctly for compressible flow. Generally, von Kármán's constant is upheld, but there is significant variance in C. Note that in the viscous sublayer, generally defined as $y^+ < 5$, the law of the wall does not accurately describe the fluid behavior. The relevant equation for this layer is found to be

$$u^+ = y^+, \tag{5}$$

and there is a smooth transition, referred to as the buffer layer, between the relationship given by Eqs. (1) and (5).

Multiple attempts to extend the law of the wall to compressible flow regimes were made, and the Van Driest I [2, 3] and II [6] transformations are typically considered the most successful. The Van Driest transformations account for the density variation throughout the boundary layer by transforming the mean compressible velocities to an effective incompressible velocity, U^+_{VD}. This effective velocity replaces the incompressible scaling in Eq. (1), and the law of the wall is once again satisfied. The Van Driest II velocity transformation [7] is

$$U^+_{VD} = \frac{u_e}{u_\tau B_1}\left\{ sin^{-1}\left(\frac{2B_1^2(u/u_e) - B_2}{\sqrt{B_2^2 + 4B_1^2}}\right) + sin^{-1}\left(\frac{B_2}{\sqrt{B_2^2 + 4B_1^2}}\right)\right\}, \tag{6}$$

where the subscript e denotes quantities at the edge of the boundary layer, and B_1 and B_2 are defined as

$$B_1 = \sqrt{\left(\frac{\gamma - 1}{2}\right) M_e^2 r \left(\frac{T_e}{T_w}\right)}, \tag{7}$$

$$B_2 = \frac{1 + \frac{\gamma-1}{2} M_e^2 r}{T_w/T_e} - 1, \tag{8}$$

where γ is the ratio of specific heats, M is the Mach number, T is the temperature, and r is the recovery factor that accounts for the partial recovery of the stagnation temperature at the wall. For turbulent flow, a common approximation [7] for the recovery factor is based on the laminar Prandtl number, Pr,

$$r = (Pr)^{1/3}. \tag{9}$$

For the work presented herein, the Van Driest II velocity transformation is denoted simply as the Van Driest (VD) transformation, and the Van Driest I transformation is not used. Several experiments and direct numerical simulation studies [8, 9] have found that the VD transformed velocity collapses data very well across a wide range of Mach numbers, even up to a Mach 47 wind tunnel test with helium as shown in Figure 2 of Marvin and Coakley [10]. However, this success is limited to cases with adiabatic wall boundary conditions. When heat transfer at the wall is introduced, the VD transformation fails to satisfactorily collapse the velocity profiles, as demonstrated in Figure 3 of Huang and Coleman [11]. This also increases errors in the skin friction computations based on log-law profiles, as some authors have noted [10, 12–16]. In general, cooling the wall tends to shift the value of U^+_{VD} upwards in the log layer [17]. In the viscous sublayer, cooling a wall results in a decreased velocity gradient. Because hypersonic vehicles are typically designed with some sort of cooling system, the VD transformations [2, 3, 6] are of limited use to predict skin friction with sufficient accuracy during the vehicle design phase.

A recent development described in the literature is a new transformation which couples the scaling of the wall-normal coordinate and the velocity [18]. Because the VD transformation scales the two independently of one another, the scaled velocity gradients dU^+_{VD}/dy^+ will not match the true velocity gradients. These velocity gradients are the source of shear stresses both in the flow and at the wall boundary, so inaccurate skin friction predictions are to be expected. The new transformation, proposed by Trettel and Larsson [19] and hereafter referred to as the TL transformation, is derived such that shear stresses within the flow are preserved. The TL transformation [19] was validated for supersonic channel flow and supersonic boundary layers. Three of the four supersonic boundary layer validation cases were lightly cooled and the fourth was strongly cooled. Trettel and Larsson found that the TL transformation either matched or performed better than the VD transformation for the lightly cooled cases, and performed significantly better for the strongly cooled case. This makes the TL transformation promising for analysis of cooled hypersonic vehicles, however, its performance has

not yet been evaluated at hypersonic Mach numbers. The TL transformation, consisting of a nondimensional velocity U_{TL}^{+} coupled with a nondimensional wall-normal distance Y^{+}, is

$$U_{TL}^{+} = \int_0^{u^+} \left(\frac{\rho}{\rho_w}\right)^{1/2} \left(1 + \frac{1}{2\rho}\left(\frac{d\rho}{dy}\right)y - \frac{1}{\mu}\left(\frac{d\mu}{dy}\right)y\right) du^{+}, \tag{10}$$

$$Y^{+} = \frac{y(\tau_w \rho)^{1/2}}{\mu}. \tag{11}$$

The original paper by Trettel and Larsson [19] should be consulted for details of the transformation derivation.

The goal of this research is to examine the performance of the TL transformation [19] relative to the VD transformation [2, 3, 6] with particular emphasis on flow conditions experienced by hypersonic vehicles. If the TL transformation is able to more satisfactorily collapse turbulent boundary layer profiles across a wide range of conditions, then it will be a more useful basis of comparison for experiments. Additionally, it could form the foundation for a more accurate skin friction prediction, just as the VD transformation [2] forms the foundation for the Van Driest skin friction formula [14]. The two transformations are compared by computing the flight conditions of a hypersonic vehicle on a representative constant dynamic pressure ascent trajectory and performing Reynolds Averaged Navier-Stokes (RANS) simulations of the turbulent flow on a flat plate at those conditions. Mach numbers studied range from Mach 2 up to 16 in increments of 2, as well as two subsonic reference cases at Mach 0.3 and 0.8. The wall boundary conditions and leading edge geometry are varied from adiabatic to isothermal and sharp to blunted. In addition, transformed velocity gradients are compared to untransformed velocity gradients to demonstrate the shear stress preserving behavior of the TL transformation.

The next section describes the methodology used, including the computational fluid dynamics (CFD) software, the numerical methods, and the grids. After that, results are presented for studies on the effects of Mach number, wall cooling, and leading edge bluntness. The final section provides a brief summary and discusses significant findings.

II. Methodology

A. Numerical Methods and Models

The CFD software used in this study is VULCAN-CFD (Viscous Upwind Algorithm for Complex Flow Analysis) [20], a multiblock, cell-centered, finite-volume solver widely used for high-speed flow simulations. In the present work, viscous simulations are done using the RANS equations [4] for thermally perfect air. The Low-Dissipation Flux-Split Scheme (LDFSS) of Edwards [21] is used, and interpolation is done using the Monotone Upstream-Centered Scheme for Conservation Laws (MUSCL) [22]. The flux limiter of van Leer [22] is used to prevent oscillations in regions near shocks. The implicit diagonalized approximate factorization (DAF) [23] time-stepping scheme is used at the beginning of the simulations in order to quickly propagate the correct qualitative behavior of the flowfield, and then the incomplete LU (ILU) [24] scheme is used in order to accelerate convergence. The present work utilizes the Menter-BSL [25] turbulence model, and a model sensitivity study was previously performed to ensure that the results are not dependent on model choice [26]. The inflow conditions used are representative of what would be encountered on an access-to-space constant dynamic pressure ascent trajectory for a hypersonic vehicle [27]. The flow is initialized on a coarse grid and then interpolated onto a fine grid after a startup period in order to speed up convergence. Iterative convergence is judged by monitoring the L_2-norm of the residuals, the percent difference between mass inflow and outflow, the integrated heat transfer $\dot{Q}$, and the integrated shear force S_x at the wall boundary. Simulations are considered iteratively converged when residuals have dropped by 6 orders of magnitude from their initial value, mass flow rate error is below 1.0×10^{-5}‰, and the integrated shear force and heat transfer at the wall boundary have remained constant to 4 significant digits for 10,000 iterations. All simulations are run on the Pleiades supercomputer at NASA Ames Research Center and maintained by the NASA Advanced Supercomputing (NAS) division.

B. Grids

Two grids are used in the present study—a flat plate with a sharp nose (SN) and a flat plate with a blunt nose (BN). Both grids are two-dimensional. The SN is Cartesian, while the BN is boundary-fitted, as shown in Figure 1. The BN leading edge has a radius of 1 mm. Both the SN and BN grids extend out to 25 meters downstream of the leading edge. This long plate length allows comparing high Mach number cases to low Mach number cases at locations with matching Reynolds numbers. Both grids are non-uniform, with more resolution at the plate than in the farfield and more

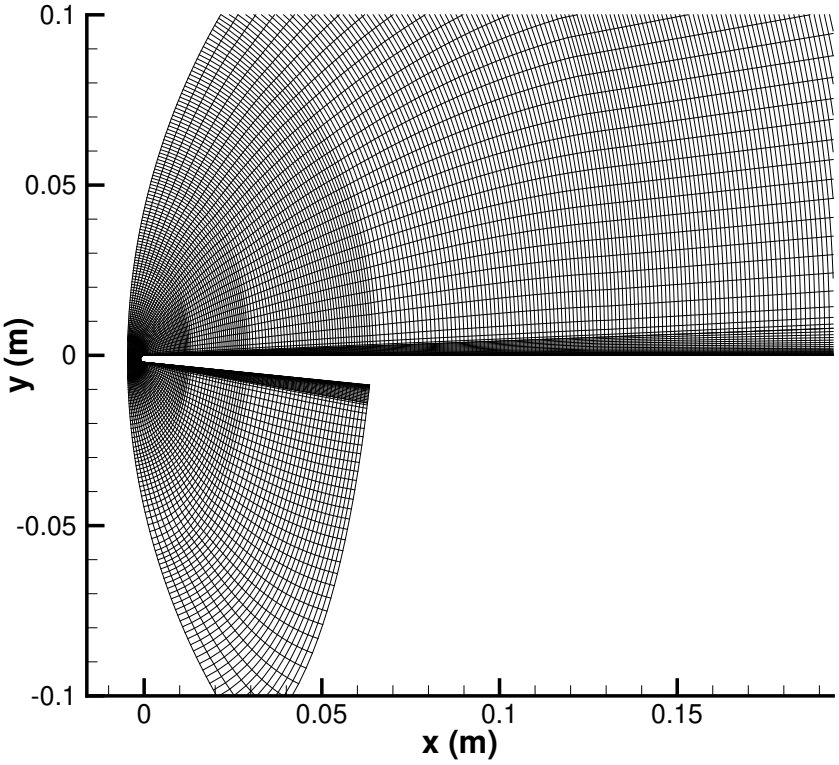

Fig. 1 Blunt nose geometry used in the present research simulations. For clarity, the coarse grid level is shown and the leading edge region is emphasized.

resolution at the leading edge than further downstream. The grids are designed such that the first y^+ values along the entire plate are less than 1.

Three grid resolution levels are used for both the SN and BN geometries: fine, medium, and coarse. A fine grid is coarsened to a medium grid by removing every other point in both dimensions. The same procedure is used to coarsen a medium grid into a coarse grid. The three resolution levels are used for a grid convergence study using the grid convergence index (GCI) of Roache [28, 29], and results are shown in Table 1 for both SN and BN meshes. The GCI, based on Richardson extrapolation [30], is calculated using two grid resolution levels and represents an estimate of the error bound between the finer resolution level and the exact solution. Quantities examined include the integrated shear force at the wall boundary, S_x, and the integrated heat transfer at the wall boundary, $\dot{Q}$. These quantities are chosen because they are calculated from points near the wall along the entire plate. This makes them a useful metric for judging near-wall resolution. Results show that three of the four quantities examined for the medium grid are within 1% of the exact value, and all quantities are within 1% of the exact value on the fine grid. Due to the small errors in the fine grid values, the fine grid is considered sufficient to achieve the stated research objectives. All results presented in the following section make use of the fine grids.

III. Results

The effect of Mach number is studied by sampling points along a representative access-to-space ascent trajectory [27] computed using a constant dynamic pressure of 1500 psf. Eight supersonic cases are selected, ranging from Mach 2 to 16 in increments of two, in addition to two subsonic reference cases at Mach 0.3 and Mach 0.8. These subsonic cases are chosen to be representative of a general aviation aircraft and a commercial transport jet, respectively. Table 2 shows the freestream conditions for each of the trajectory cases considered, where p is the ambient static pressure and

Table 1 Numerical results of the grid convergence study for both the sharp nose and blunt nose geometries.

	Coarse-Medium GCI (%)	Medium-Fine GCI (%)
SN S_x	0.477	0.260
SN $\dot{Q}$	0.083	0.066
BN S_x	1.101	0.602
BN $\dot{Q}$	0.744	0.513

the subscript 0 denotes a total, or stagnation, quantity. As a consequence of basing the simulation input conditions on a constant dynamic pressure ascent trajectory, the unit Reynolds number Re',

$$Re' = \frac{\rho_\infty u_\infty}{\mu_\infty}, \tag{12}$$

where the subscript ∞ denotes a freestream quantity, varies by roughly an order of magnitude across the cases, as shown in Figure 2. Thus, to ensure a meaningful comparison of results, all simulations are compared at matching values of Re^*_τ, proposed by Trettel and Larsson [19] as

$$Re^*_\tau = \frac{\rho_e(\tau_w/\rho_e)^{1/2}\delta}{\mu_e}, \tag{13}$$

where δ is the boundary layer thickness. The Re^*_τ value used in the present study is 3000. The effect of cooling is studied by holding the wall boundary to a fixed temperature such that some representative engineering materials will not melt from the high temperatures produced by hypersonic flight. The chosen wall temperatures, T_W, for isothermal cases are shown in Table 2. A side effect of holding the wall temperature constant is that the resulting heat flux will vary as the vehicle Mach number increases. Thus, the effect of cooling becomes more pronounced at higher Mach numbers. Finally, the leading edge bluntness for BN cases is chosen to have a nose radius of 1 mm in order to be broadly representative of the curvature found on the nose of hypersonic vehicles. The X-43A Mach 7 vehicles had leading edge nose radii of 0.762 mm, while the Mach 10 vehicle had a leading edge nose radius of 1.27 mm [31].

Table 2 Simulation input conditions from ascent trajectory analysis.

M_∞	Alt (km)	$p_0(kPa)$	$\rho_\infty(\frac{kg}{m^3})$	$U_\infty(\frac{m}{s})$	$T_\infty(K)$	$T_0(K)$	$T_W(K)$
0.3	0.30	1.040e+05	1.190	101.7	286.2	291.3	300
0.8	9.14	4.587e+05	4.583e-01	242.5	228.7	258.0	240
2.0	10.20	2.007e+05	4.027e-01	597.2	221.9	399.4	380
4.0	19.00	9.736e+05	1.031e-01	1180.3	216.6	909.4	800
6.0	24.18	4.500e+06	4.496e-02	1787.4	220.8	1810.8	1200
8.0	27.93	1.565e+07	2.487e-02	2403.4	224.6	3099.2	1200
10.0	30.88	4.354e+07	1.571e-02	3023.9	227.5	4778.2	1200
12.0	33.33	1.029e+08	1.068e-02	3667.1	232.4	6924.9	1200
14.0	35.46	2.156e+08	7.652e-03	4332.7	238.3	9580.7	1200
16.0	37.34	4.119e+08	5.732e-03	5006.2	243.6	12715.9	1200

A. Effect of Mach Number

Figures 3(a) and 3(b) show the VD [6] transformed velocity and the TL [19] transformed velocity as functions of the transformed wall-normal coordinate, respectively. The curve denoted by "LotW Theory" represents the incompressible law of the wall [5] result. The remaining curves denote the simulation cases corresponding to the sharp nose flat plate

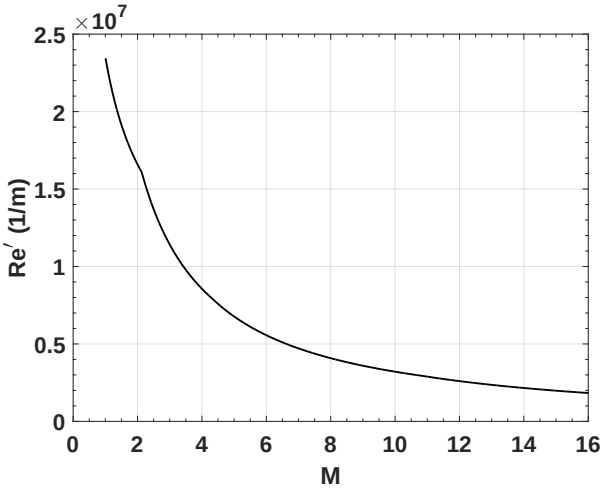

Fig. 2 Unit Reynolds number as a function of Mach number.

with adiabatic wall boundary conditions and varying Mach numbers. For the Van Driest transformation, departure from collapse can first be observed in the buffer layer. At $y^+ = 10$, the cases at Mach 6 and below are seen to collapse onto one another, but the higher Mach number cases begin to diverge. Near the end of the buffer layer at $y^+ = 30$, the Mach 6 case is seen to be departing as well, and there are significant differences between the higher Mach number cases and the collapsed cases. In the log layer, the Mach 4 case begins to depart at $y^+ \approx 100$, and the Mach 2 case departs from the subsonic reference cases at $y^+ \approx 700$. It is worth noting that although Reynolds number effects are controlled by matching Re^*_τ for the different cases, differences in the wake parameters [32, 33] are not controlled. This wake effect is leading to some of the discrepancy seen in the VD transformation results.

The TL transformation [19], shown in Figure 3(b), shows generally improved performance compared to the VD transformation. Within the buffer layer at $Y^+ = 10$, all of the cases collapse onto one another. Near the end of the buffer layer at $Y^+ = 30$, some slight fanning out can be observed, comparable to what is seen for the VD transformation at $y^+ = 10$. This demonstrates an improvement for conditions of increasing Mach number with an adiabatic wall boundary. The Mach 6 case does not differ significantly from the collapsed cases until $Y^+ \approx 300$, and the Mach 4 case not until $Y^+ \approx 500$. Mach 2 does not depart from the subsonic reference cases within the bounds of the plot. These results indicate that the TL transformation shows an improved ability to collapse turbulent boundary layer velocity profiles compared to the VD transformation across widely varying Mach numbers.

B. Effect of Wall Cooling

Figure 4 shows the two transformations when cooling is applied at the wall. As with Figure 3, the curve denoted with "LotW Theory" indicates the incompressible law of the wall [5] result, while the remaining curves denote the simulation cases corresponding to the sharp nose flat plate with isothermal wall boundary conditions and varying Mach numbers. As discussed previously, a result of the choice of fixed wall temperature is that the cooling must increase as the Mach number increases. For the VD transformation [6], shown in Figure 4(a), departure from collapse is now visible in the viscous sublayer as close to the wall as $y^+ = 3$. The Mach 8 case is seen to diverge from the collapsed lower Mach number cases by $y^+ \approx 10$, and the Mach 6 case departs by $y^+ \approx 200$. Furthermore, it is observed that the cases at Mach 10 and higher do not have the correct slope throughout the log layer, with the Mach 16 case showing the largest error.

For the TL transformation [19], shown in Figure 4(b), all of the Mach number cases collapse onto one another throughout the viscous sublayer. Departure from collapse is just beginning to occur for the cases at Mach 10 and above as $Y^+ = 10$ is approached. Although there is not a very good collapse throughout the log layer, the curves do generally have the correct slope, unlike the Van Driest transformed [6] velocities. These results indicate that the VD transformation is missing some of the essential physics in the viscous sublayer that the TL transformation is able to capture. The improved performance of the TL transformation is due to coupling the velocity transformation with the wall-normal coordinate transformation in such a way that shear stresses are preserved and momentum is conserved.

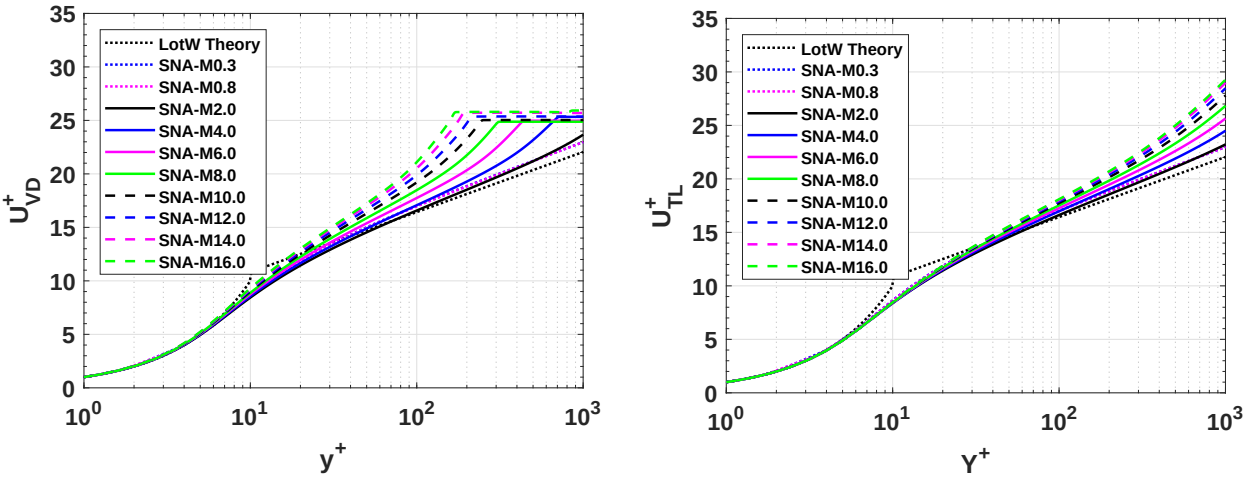

(a) VD transformation. (b) TL transformation.

Fig. 3 Effect of Mach number on the sharp nose adiabatic (SNA) cases from Mach 0.3 to Mach 16.

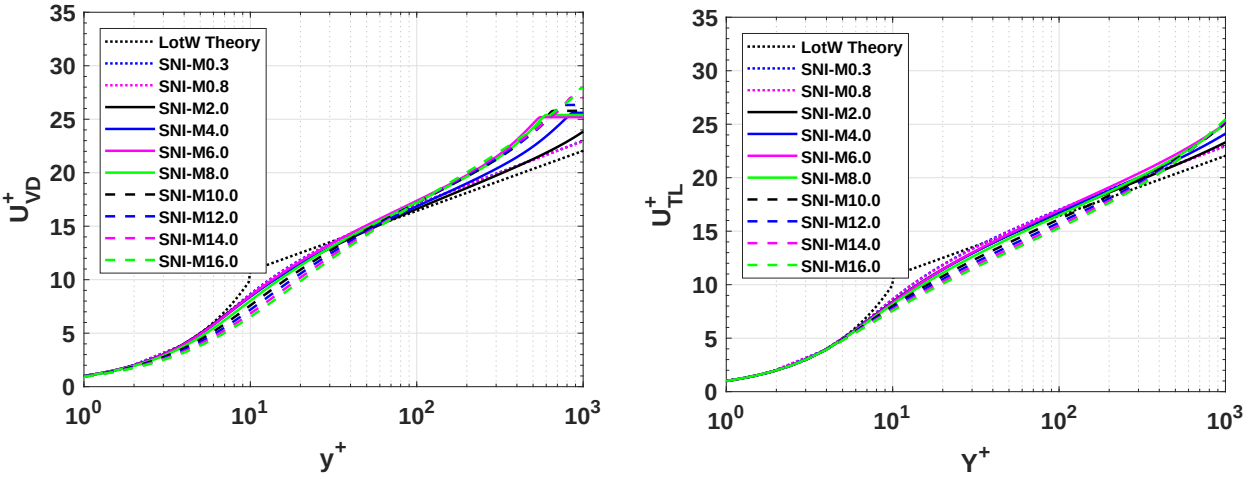

(a) VD transformation. (b) TL transformation.

Fig. 4 Effect of wall cooling on the sharp nose isothermal (SNI) cases from Mach 0.3 to Mach 16.

C. Effect of Leading Edge Shape

Figure 5 shows the effect that leading edge shape has on transformation performance. Results for the VD transformation [6] are shown in Figure 5(a) and results for the TL transformation [19] are shown in Figure 5(b). Once again, the incompressible law of the wall [5] result is denoted by "LotW Theory" and the curves denoted by BNI correspond to simulation cases using the blunt nose geometry with isothermal wall boundary conditions and varying Mach numbers. Leading edge shape does not appear to have a strong impact on transformation performance, as the results shown in Figure 5 are very similar to the results shown in Figure 4. As with the wall cooling study, departure from collapse can first be observed around $y^+ \approx 3$ for the VD transformation. The Mach 8 case once again departs from the lower Mach number cases by $y^+ \approx 10$, while the Mach 6 case departs by $y^+ \approx 200$. Finally, discrepancy can be seen between the Mach 4 case and the lower Mach number collapsed cases at $y^+ = 300$. These results show that the VD transformation performance with a blunted leading edge nearly mirrors that found for a sharp leading edge in Figure 4(a).

When the TL transformation [19] is applied to a blunt leading edge geometry, shown in Figure 5(b), the results are similar to those found for a sharp leading edge. All of the cases up to Mach 16 collapse onto one another in the viscous sublayer, and discrepancies do not appear until the buffer layer is reached. The cases at Mach 10 and above again begin to diverge from the other cases at around $Y^+ \approx 10$, but the correct slope is generally maintained throughout the log layer.

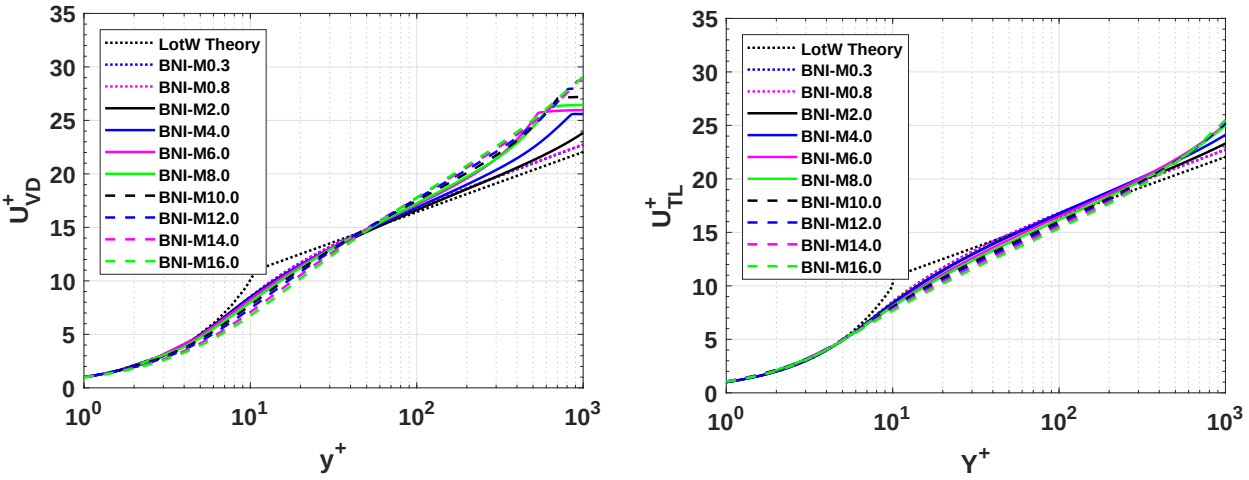

(a) VD transformation.

(b) TL transformation.

Fig. 5 Effect of leading edge bluntness on the blunt nose isothermal (BNI) cases from Mach 0.3 to Mach 16.

Although the results of the blunt leading edge cases are very similar to the sharp leading edge cases, they are not identical. This is because the primary effect of blunting the nose, at least for a small radius as considered in the present research, is a detached bow shock in front of the plate. The sharp nose cases, in comparison, have a weak Mach wave coming off the leading edge. If the unit Reynolds numbers are compared after both types of waves, their numerators are identical due to continuity. However, bow shocks cause larger increases in pressure and temperature than Mach waves do. The increased temperature after the bow shock results in a higher viscosity, and therefore a lower unit Reynolds number, than after the Mach wave. Although the present study holds Re^*_τ fixed, there are small differences in other Reynolds numbers between the sharp nose and the blunt nose. Those differing Reynolds numbers will cause some subtle changes in the velocity profiles. Although these differences are perceptible in the VD transformed velocity profiles, they are not noticeable in the TL transformed profiles.

D. Nondimensional Velocity Gradients

Although improvement can be seen in the TL transformation [19] compared to the VD transformation [6] in Figures 3-5, the mean velocity profile plots cannot provide an explanation for this enhanced performance. The reason for the observed improved performance is primarily due to shear stresses and velocity gradients. In the Van Driest transformation, the velocity and the wall-normal coordinate are scaled independently from one another. Because different scaling factors are used for the velocity and the wall-normal coordinate, the transformed velocity gradients are distorted compared to the untransformed gradients. As distance from the wall increases, this error in the velocity gradients accumulates into error in the integrated velocity profile. In contrast to this, the TL transformation couples the scaling of the velocity and the wall-normal coordinate together by including a shear stress balance in its derivation. The result is that the transformed velocity gradients match the untransformed normalized velocity gradients. As the distance from the wall increases, the matching velocity gradients are integrated and the mean velocity profiles more closely match one another.

Figure 6 shows both the VD [6] and TL [19] transformed velocity gradients compared to the untransformed true velocity gradients normalized by μ/τ_w. For clarity, one out of every eight grid points is shown for the normalized true velocity gradients. Results are shown for Mach numbers 6 and 10, for both adiabatic and isothermal boundary conditions. Comparing Figure 6(a) to 6(c) shows that increasing the Mach number while maintaining an adiabatic boundary condition increases the amount that the VD transformed velocity gradients deviate from the true velocity gradients. The VD transformed velocity gradients are seen to begin departing from the normalized true gradients as close to the wall as $Y^+ = 2$. This is in accordance with the earlier observation that the VD transformation is not capturing all of the essential physics within the viscous sublayer. Comparing Figure 6(a) to 6(b) shows that when cooling is applied at the wall through an isothermal boundary condition, the VD transformed velocity gradients tend to decrease. As the degree of cooling increases, as in the Mach 10 cases of Figures 6(c) and 6(d), the decrease in VD

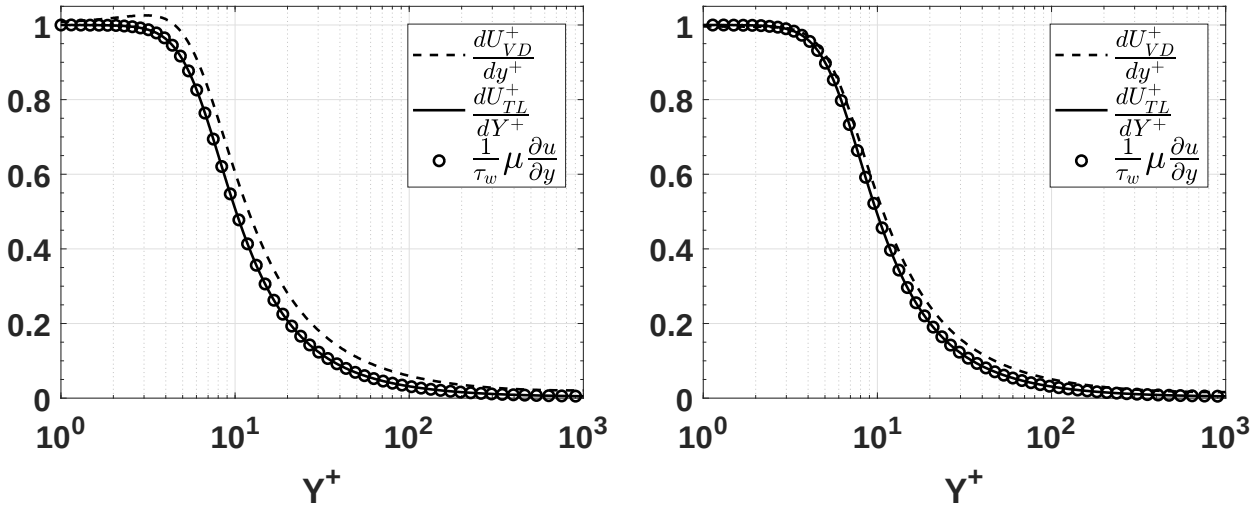

(a) SNA Mach 6.0.

(b) SNI Mach 6.0.

(c) SNA Mach 10.0.

(d) SNI Mach 10.0.

Fig. 6 Comparison of the nondimensional velocity gradients of the VD and TL transformations with the normalized velocity gradients.

transformed velocity gradients is greater. For all Mach numbers and wall boundary conditions examined in the present study, the TL transformed velocity gradients match the normalized true velocity gradients perfectly.

IV. Conclusion

The Van Driest transformation, despite being a standard technique in the analysis of compressible flows, is known to have some shortcomings. A transformation proposed by Trettel and Larsson shows promise for rectifying these deficiencies. The stated objective of this study is to examine the performance of the transformation of Trettel and Larsson relative to the Van Driest transformation for flows characteristic of those found in the analysis of hypersonic flight vehicles, featuring both high Mach numbers and significant cooling at the wall. The TL transformation is shown to collapse mean velocity profiles more satisfactorily than the VD transformation, particularly in the viscous sublayer and buffer region. This improved performance is maintained whether the wall boundary condition is adiabatic or isothermal, and appears to be independent of leading edge geometry. Velocity gradients of the TL transformation are also shown to match the true velocity gradients when they are normalized using viscosity and the wall shear stress.

References

[1] Von Kármán, T., "Mechanical Similitude and Turbulence," *NACA Technical Memorandum*, 1931.

[2] Van Driest, E. R., "Turbulent Boundary Layer in Compressible Fluids," *Journal of the Aerospace Sciences*, Vol. 18, 1951, pp. 145–160.

[3] Van Driest, E. R., "Turbulent Boundary Layer in Compressible Fluids," *Journal of the Aeronautical Sciences*, 2012.

[4] Wilcox, D. C., et al., *Turbulence Modeling for CFD*, Vol. 3, DCW industries La Canada, CA, 2006.

[5] Pope, S. B., *Turbulent Flows*, Cambridge University Press, 2000. doi:10.1017/CBO9780511840531.

[6] Van Driest, E. R., "The Problem of Aerodynamic Heating," *Aeronautical Engineering Review*, Vol. 15, 1956, pp. 26–51.

[7] Schetz, J. A., and Bowersox, R. D. W., "Boundary Layer Analysis," , 2011.

[8] Maeder, T., "Numerical Investigation of Supersonic Turbulent Boundary Layers," Ph.D. thesis, Swiss Federal Institute of Technology Zürich, 2000.

[9] Duan, L., Beekman, I., and Martin, M., "Direct Numerical Simulation of Hypersonic Turbulent Boundary Layers. Part 3. Effect of Mach Number," *Journal of Fluid Mechanics*, Vol. 672, 2011, pp. 245–267.

[10] Marvin, J. G., and Coakley, T., "Turbulence Modeling for Hypersonic Flows," *NASA STI/Recon Technical Report N*, Vol. 89, 1989.

[11] Huang, P., and Coleman, G. N., "Van Driest Transformation and Compressible Wall-Bounded Flows," *AIAA journal*, Vol. 32, No. 10, 1994, pp. 2110–2113.

[12] Hopkins, E. J., "Charts for Predicting Turbulent Skin Friction from the Van Driest Method (2)," *NASA Technical Report*, 1972.

[13] Hopkins, E. J., and Inouye, M., "An Evaluation of Theories for Predicting Turbulent Skin Friction and Heat Transfer on Flat Plates at Supersonic and Hypersonic Mach Numbers," *AIAA Journal*, Vol. 9, No. 6, 1971, pp. 993–1003.

[14] Bradshaw, P., "An Improved Van Driest Skin-Friction Formula for Compressible Turbulent Boundary Layers," *AIAA Journal*, Vol. 15, No. 2, 1977, pp. 212–214.

[15] Bradshaw, P., "Compressible Turbulent Shear Layers," *Annual Review of Fluid Mechanics*, Vol. 9, No. 1, 1977, pp. 33–52.

[16] Huang, P., Bradshaw, P., and Coakley, T., "Skin Friction and Velocity Profile Family for Compressible Turbulent Boundary Layers," *AIAA journal*, Vol. 31, No. 9, 1993.

[17] Danberg, J. E., "Characteristics of the Turbulent Boundary Layer with Heat and Mass Transfer at M = 6.7," Ph.D. thesis, Catholic University of America, 1964.

[18] Trettel, A., "Velocity transformation for compressible wall turbulence with heat transfer," Master's thesis, University of Maryland, College Park, 2015.

[19] Trettel, A., and Larsson, J., "Mean Velocity Scaling for Compressible Wall Turbulence with Heat Transfer," *Physics of Fluids*, Vol. 28, No. 2, 2016, p. 026102.

[20] Baurle, R., "VULCAN-CFD," `https://vulcan-cfd.larc.nasa.gov/`, 2018.

[21] Edwards, J. R., "A Low-Diffusion Flux-Splitting Scheme for Navier-Stokes Calculations," *Computers & Fluids*, Vol. 26, No. 6, 1997, pp. 635–659.

[22] Van Leer, B., "Towards the Ultimate Conservative Difference Scheme. II. Monotonicity and Conservation Combined in a Second-Order Scheme," *Journal of Computational Physics*, Vol. 14, No. 4, 1974, pp. 361–370.

[23] Pulliam, T. H., and Chaussee, D., "A Diagonal Form of an Implicit Approximate-Factorization Algorithm," *Journal of Computational Physics*, Vol. 39, No. 2, 1981, pp. 347–363.

[24] Chan, T. F., and Van der Vorst, H. A., "Approximate and Incomplete Factorizations," *Parallel Numerical Algorithms*, Springer, 1997, pp. 167–202.

[25] Menter, F. R., et al., "Two-Equation Eddy-Viscosity Turbulence Models for Engineering Applications," *AIAA journal*, Vol. 32, No. 8, 1994, pp. 1598–1605.

[26] DiGregorio, N. J., "Characteristics of Turbulent Boundary Layers Along a Hypersonic Vehicle," Master's thesis, State University of New York at Buffalo, 2018.

[27] Heiser, W. H., and Pratt, D. T., *Hypersonic Airbreathing Propulsion*, AIAA, 1994.

[28] Roache, P. J., "Perspective: A Method for Uniform Reporting of Grid Refinement Studies," *Transactions-American Society of Mechanical Engineers Journal of Fluids Engineering*, Vol. 116, 1994, pp. 405–405.

[29] Roache, P. J., "Quantification of Uncertainty in Computational Fluid Dynamics," *Annual Review of Fluid Mechanics*, Vol. 29, No. 1, 1997, pp. 123–160.

[30] Richardson, L. F., J Arthur Gaunt, B., et al., "VIII. The Deferred Approach to the Limit," *Phil. Trans. R. Soc. Lond. A*, Vol. 226, No. 636-646, 1927, pp. 299–361.

[31] Ohlhorst, C. W., Glass, D. E., Bruce III, W. E., Lindell, M. C., Vaughn, W. L., Dirling Jr, R., Hogenson, P., Nichols, J., Risner, N., and Thompson, D., "Development of X-43A Mach 10 Leading Edges," *56th International Astronautical Congress*, Fukuoka, Japan, 2005.

[32] Coles, D., "The Law of the Wake in the Turbulent Boundary Layer," *Journal of Fluid Mechanics*, Vol. 1, No. 2, 1956, pp. 191–226.

[33] Chauhan, K. A., Monkewitz, P. A., and Nagib, H. M., "Criteria for Assessing Experiments in Zero Pressure Gradient Boundary Layers," *Fluid Dynamics Research*, Vol. 41, No. 2, 2009, p. 021404.